Research in Astron. Astrophys. **2013** Vol. **13** No. **7**, 783–802
http://www.raa-journal.org *http://www.iop.org/journals/raa*

Research in Astronomy and Astrophysics

Model fitting of the kinematics of ten superluminal components in blazar 3C 279

Shan-Jie Qian

National Astronomical Observatories, Chinese Academy of Sciences, Beijing 100012, China; *rqsj@bao.ac.cn*

Received 2012 October 28; accepted 2013 February 26

Abstract The kinematics of ten superluminal components (C11– C16, C18, C20, C21 and C24) of blazar 3C 279 are studied from VLBI observations. It is shown that their initial trajectory, distance from the core and apparent speed can be well fitted by the precession model proposed by Qian. Combined with the results of the model fit for the six superluminal components (C3, C4, C7a, C8, C9 and C10) already published, the kinematics of sixteen superluminal components can now be consistently interpreted in the precession scenario with their ejection times spanning more than 25 yr (or more than one precession period). The results from model fitting show the possible existence of a common precessing trajectory for these knots within a projected core distance of $\sim$0.2–0.4 mas. In the framework of the jet-precession scenario, we can, for the first time, identify three classes of trajectories which are characterized by their collimation parameters. These different trajectories could be related to the helical structure of magnetic fields in the jet. Through fitting the model, the bulk Lorentz factor, Doppler factor and viewing angle of these knots are derived. It is found that there is no evidence for any correlation between the bulk Lorentz factor of the components and their precession phase (or ejection time). In a companion paper, the kinematics of another seven components (C5a, C6, C7, C17, C19, C22 and C23) have been derived from model fitting, and a binary black-hole/jet scenario was envisaged. The precession model proposed by Qian would be useful for understanding the kinematics of superluminal components in blazar 3C 279 derived from VLBI observations, by disentangling different mechanisms and ingredients. More generally, it might also be helpful for studying the mechanism of jet swing (wobbling) in other blazars.

Key words: radio continuum — galaxies: jets — galaxies: kinematics — galaxies: individual (blazar 3C 279)

1 INTRODUCTION

Research on blazars is an important extragalactic astrophysical field, in which extensive observations of their radiation from radio to γ-ray are carried out, and the mechanisms of radiation are studied (recent progress can be seen in: e.g., Marscher et al. 2011; Marscher & Jorstad 2011; Abdo et al. 2010; Raiteri et al. 2010; Schinzel et al. 2010; Velcellone et al. 2010; Marscher et al. 2010; Qian 2011, 2012).

Quasar 3C 279 ($z = 0.538$) is one of the most well studied prominent blazars (or flat-spectrum compact radio sources, many of which display superluminal motion). It is an optically violent variable quasar with large and rapid polarized outbursts and it radiates across the entire electromagnetic spectrum from radio through optical and X-ray to γ-rays. Very strong variability is observed in all these wavebands with various timescales (hours/days to years).

3C 279 was one of the brightest EGRET quasars (Hartman et al. 1992). Since the Fermi satellite was launched in 2008, further investigations of 3C 279 have been made (e.g. Abdo et al. 2010; Marscher et al. 2012). Multifrequency observations, studies of its spectral energy distribution and correlations between different wavebands have demonstrated important clues about the radiation mechanisms, especially for X-ray and γ-ray emission and their emission positions in the jet (Jorstad et al. 2007; Marscher 2008, 2009; Marscher & Jorstad 2011; Marscher et al. 2011; Abdo et al. 2010; Chatterjee et al. 2012).

Recently, correlations between outbursts in γ-ray, X-ray, optical/IR and ejection of superluminal components in 3C 279 have been intensively studied, which have provided important information (e.g. Chatterjee et al. 2012; Abdo et al. 2010).

3C 279 is the first object in which superluminal motion was detected (Whitney et al. 1971; Cohen et al. 1971) and structure and kinematics have been monitored by using very long baseline interferometry (VLBI). Numerous data have been presented in the literature on the kinematics and evolution of flux polarization in superluminal knots.

VLBI observations reveal that bright components (knots) are consistently ejected from a core (presumed to be stationary) and move away from it with apparent superluminal speeds ($\sim$4–20c where c is the speed of light, Jorstad & Marscher 2005; Jorstad et al. 2004; Homan et al. 2003; Wehrle et al. 2001; Carrara et al. 1993; Unwin et al. 1989; Chatterjee et al. 2008; Larionov et al. 2008; Qian 2012). Recently, Jorstad et al. (2012) observed two superluminal knots K2 and K3, whose appearance in the jet was accompanied by an increase in flux and fractional polarization of the core. The knots had apparent speeds of $16.3\pm2.0c$ and $19.7\pm2.0c$, respectively, and their time of passage through the mm-wave core coincided with the two most prominent events in the γ-ray light curve, in Dec. 2008–Apr. 2009 and in Autumn 2010. The apparent superluminal motion resulted from relativistic motion of the knots at small viewing angles and the flux density or luminosity of the knots was strongly Doppler-boosted. Thus the determination of their intrinsic flux (luminosity) and variation is only possible when their Doppler factor was measured (Qian et al. 1996; Steffen et al. 1995).

High resolution VLBI observations have revealed swings in the ejection position angle of superluminal components in several blazars, see Stirling et al. (2003, BLLac); Bach et al. (2005, S5 0716+714); Savolainen et al. (2006, 3C 273); Agudo et al. (2007, NRAO 150); Lobanov & Roland (2005, 3C 345); Qian et al. (2009, 3C 345). Although the physical origin of this phenomenon is poorly understood, it may be important for studying the relation between the formation of the relativistic jet and the supermassive black hole/accretion disk system. In blazar 3C 279, the swing of the projected position angle of the superluminal components has been observed with an amplitude of about 60°, but the behavior is much more complex (see, e.g., Chatterjee et al. 2008; Qian 2011, 2012). It seems very difficult to judge whether the swing could be regular (due to precession) or not (due to instability), or if different mechanisms could play roles together. Some indication of ejection of superluminal components during precession has been pointed out by Jorstad & Marscher (2005), based on the variation of the observed apparent speeds for the components C1 (ejected in epoch $\sim$1968) to C20 (ejected in epoch $\sim$2003.4). A precession period of $\sim$31 yr was suggested.

Since it seems difficult to propose a unified model that incorporates precession which can interpret the kinematic behavior of all these superluminal components in 3C 279, Qian (2011, 2012) has proposed a specific precession model to fit the kinematics for as many components as possible and try to discover the causes for those components deviating from the predictions of the precession model. The precession model with a 25 year period proposed by Qian (2011) is based on a VLBI

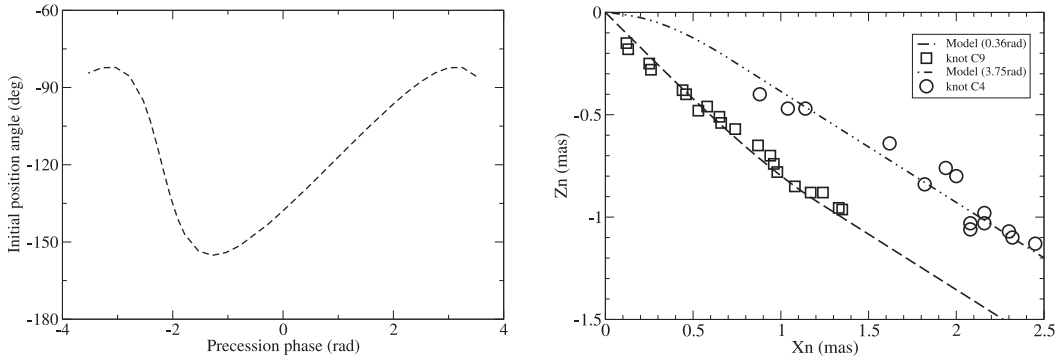

Fig. 1 Relation between the initial (or ejection) position angle and the precession phase (ϕ) given by the precession model (Qian 2011) (*left panel*) and the fits to the model of the observed trajectory of knots C4 and C9 (Qian 2012), with their precession phase and ejection time differing by 3.4 rad and 13.5 yr (more than half of the precession period of 25 yr), respectively (*right panel*).

dataset that spans 30 yr and has well fitted the kinematics of six superluminal components (C3, C4, C7a, C8, C9 and C10), as described in Qian (2012).

Figure 1 shows the relation between the initial position angle (IPA) and the precession phase (left panel) that was derived from the model, and the model fits to the trajectory of knots C4 and C9. Their ejection times differed by 13.5 years (or a phase difference of 3.4 rad; right panel). Both fits of the kinematics for knots C4 and C9 are very good. The fit to the trajectory of knot C9 shown in Figure 1 (right panel) is an example. In particular, the derived parameters (bulk Lorentz factor, Doppler factor and viewing angle) for knot C4 are remarkably consistent with the VLBI observations conducted by Homan et el. (2003). The fits to the model can not only explain the change in its apparent speed associated with the curvature of the trajectory due to the change in viewing angle, but can also explain the change in its flux density, taking into account the increase of its angular size and decrease of its Doppler factor after the occurrence of curvature (Qian et al. 2010).

In this paper, we fit the model to the kinematics, including initial trajectory, core distance and apparent velocity, of ten more components (C11–C16, C18, C20, C21 and C24) using the precession scenario. Although these results are still not enough to confirm the existence of precession, they are helpful for understanding the behavior of superluminal components in 3C 279 from VLBI observations.

In a companion paper we will discuss the fitting of the kinematics of another seven components (C5a, C6, C7, C17, C19, C22 and C23) with the model and envisage a binary black-hole/jet scenario.

The data used for the fittings to the model are mostly collected from the 43 GHz VLBI observations by Chatterjee et al. (2008), Jorstad et al. (2004) and Larionov et al. (2008). The data typically have observational errors of $\sim \pm 0.01 - 0.03$ mas in coordinates, $\sim \pm 0.03$–0.06 mas in core distance and $\sim \pm 4 - 8^\circ$ in position angle. They are good enough for our study to tentatively demonstrate the possible precession behavior in the source.

In this paper, we will adopt the concordant cosmological model (ΛCDM model) with $\Omega_m = 0.3$, $\Omega_\lambda = 0.7$ and Hubble constant $H_0 = 70$ km s^{-1} Mpc^{-1} (Spergel et al. 2003). Thus for 3C 279, $z = 0.538$, its luminosity distance is D_l= 3.096 Gpc (Hogg 1999; Pen 1999) and angular diameter distance D_a=1.309 Gpc. The angular scale of $1\,\mathrm{mas} = 6.35\,\mathrm{pc}$, and the proper motion of 1 mas yr^{-1} is equivalent to an apparent velocity of 31.81 c.

2 FORMALISM OF THE MODEL

The formalism of the precession model has been described in detail in Qian (2011). We do not want to fully describe the geometry of the model (referring to fig. 1 in that paper), but only recall the expressions for the amplitude of the collimated path and the precession phase, and the equations for calculating the apparent velocity, Doppler factor and elapsed time. The fitting techniques have been described in detail in Qian (2012).

In order to fit the initial (ejection) position angle and the initial part of the trajectory[1] for as many knots as possible, we have to try to find an appropriate set of model parameters and functions to describe the amplitude and precession phase of their trajectory.

The trajectory of a knot is described in cylindrical coordinates ($z(t)$, $A(t)$, $\Phi(t)$), where $z(t)$ is the distance from the origin of the coordinate system along the precession axis (z-axis)[2]. The precession axis is defined by parameters ϵ and ψ (see Qian 2011). $A(z)$ is the amplitude of the path and $\Phi(z)$ is the azimuthal angle. A and z are measured in units of mas.

Amplitude (A) as a function of z is taken such that when $z \leq c2$, where $c2$ is always less than $b = 50$ mas as given in the original model by Qian (2012),

$$A(z) = \frac{2b}{\pi} 1.375 \times 10^{-2} \sin\left(\frac{\pi z}{2b}\right) , \tag{1}$$

when $z > c2$,

$$A(z) = \frac{2b}{\pi} 1.375 \times 10^{-2} \sin\left(\frac{\pi c2}{2b}\right) \left[1 - \frac{z - c2}{c3}\right] . \tag{2}$$

In the following fittings to the model, Equation (1) is used to describe the amplitude function for knots C11, C18, C20, C21 and C24 for which parameter $c2 > 20$ mas. For knots C12, C13, C14, C15 and C16, both Equations (1) and (2) are used to describe their amplitude functions which are shown in Figure 2. Their $c2$ and $c3$ are given in Table 1. Thus we have different collimation/curvature distances (parameter $c2$) for different knots: 50 pc (C12); 57 pc (C13); 76 pc (C14); 64 pc (C15) and 76 pc (C16), in comparison with 320 pc (50 mas) for knots C4 and C9. Parameter $c3$ is not sensitive to the fitting of the model and is given relatively arbitrarily.

Table 1 Parameters $c2$ and $c3$ for defining the amplitude functions for superluminal knots C12–C16.

Knot	$c2$ (mas)	$c2$ (pc)	$c3$ (mas)
C12	8	50	1200
C13	9	57	500
C14	12	76	500
C15	10	64	500
C16	12	76	12 000

The precession phase is given by

$$\Phi(z) = \Phi_0 + \phi , \tag{3}$$

where Φ_0 is taken to be 3.783 rad (arbitrary) and ϕ is defined as the precession phase. Thus the trajectory of an individual knot is described by ($A(z)$, ϕ = const.) which represent a collimated jet trajectory. Correspondingly, when $z \leq c2$,

$$\frac{dA}{dz} = 1.375 \times 10^{-2} \cos\left(\frac{\pi z}{2b}\right) , \tag{4}$$

[1] We designate the portion of the observed trajectory within a core distance of ∼0.2–0.4 mas as the "initial trajectory."

[2] In the following figures, coordinates (X_n, Z_n) are defined to be relative right ascension and relative declination, respectively, in units of mas ($1\,\mathrm{mas} = 6.35\,\mathrm{pc}$).

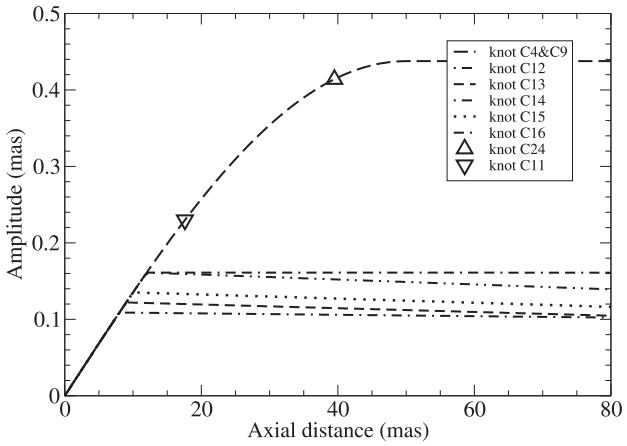

Fig. 2 Amplitude functions for knots C12, C13, C14, C15 and C16 are represented with different lines, as shown in the legend in the top right corner of the figure (see Table 1). The amplitude function of the original model (Qian 2011, 2012) is shown by the bold dashed curve (for knots C4 and C9), on which the up-pointing triangle and down-pointing triangle represent the observed maximum axial distance of knots C24 and C11, respectively. The collimation/curvature of the trajectory for knots C12 to C16 is assumed to occur at distances much closer to the core than that of the original model for knots C4 and C9 with collimation parameter $b = 50$ mas.

when $z > c2$,

$$\frac{dA}{dz} = -1.375 \times 10^{-2} \left(\frac{2b}{\pi}\right) \sin\left(\frac{\pi c2}{2b}\right) / c3\,. \tag{5}$$

We also have

$$\frac{d\Phi}{dz} = 0\,, \tag{6}$$

and

$$\Delta = \arctan\left(\frac{dA}{dz}\right), \tag{7}$$

$$\Delta_p = \arctan\left(\frac{dA}{dz}\sin\Phi\right), \tag{8}$$

$$\cos\Delta_s = \left[1 + \left(\frac{dA}{dz}\right)^2\right]^{-1/2}. \tag{9}$$

From Equation (4), we obtain the half opening angle of the precession cone to be $\eta = 0.79°$. The formulas for viewing angle θ, apparent transverse velocity $\beta_{\rm a}$, Doppler factor δ and elapsed time T_0 when the knot reaches distance z are given as follows.

$$\theta = \arccos[\cos\epsilon(\cos\Delta + \sin\epsilon\tan\Delta_p)]\,, \tag{10}$$

$$\delta = \frac{1}{\Gamma(1-\beta\cos\theta)}\,, \tag{11}$$

$$\beta_{\rm a} = \frac{\beta\sin\theta}{1-\beta\cos\theta}\,, \tag{12}$$

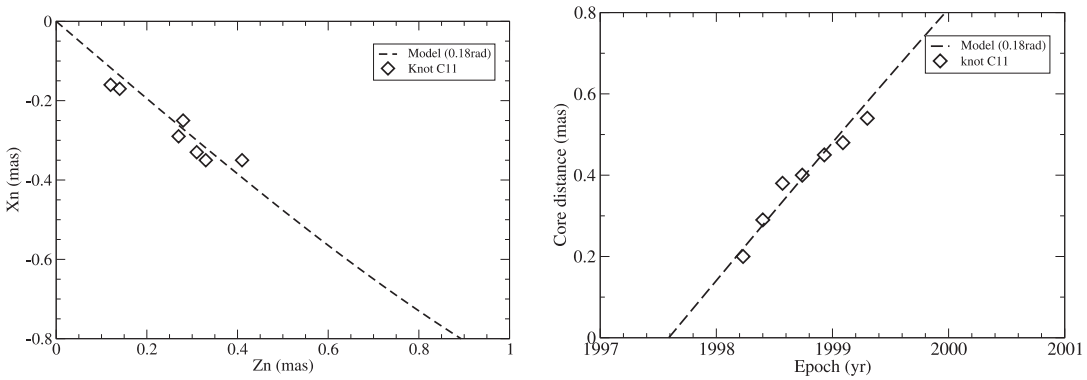

Fig. 3 Model fit of the trajectory (*left panel*) and core distance (*right panel*) of knot C11.

$$T_0 = \int_0^z \frac{1+z'}{\Gamma\delta v \cos\Delta_s} dz\,. \tag{13}$$

Here z' is redshift, $\beta = v/c$ and v is the spatial velocity of the knot; $\Gamma = (1-\beta^2)^{-1/2}$ is the Lorentz factor.

As in the original precession model (Qian 2011, 2012) we adopt the parameters $\epsilon = 1.32^\circ$ and $\psi = 28.53^\circ$, which define the direction of the precession axis. Thus the initial viewing angle (IVA) changes between 0.53° and 2.11°.

3 FITTING THE KINEMATICS OF TEN KNOTS (C11–C16, C18, C20, C21 AND C24) WITH THE MODEL

In the following we will discuss the individual model fitting for each of these superluminal knots.

3.1 Model Fitting of the Kinematics of Knot C11

We take the following parameters: ejection epoch $t_0 = 1997.59$, precession phase $\phi = 0.18$ rad and bulk Lorentz factor $\Gamma = 14.0$. Correspondingly we obtain: IPA $= -134.3^\circ$ and IVA $= 1.97^\circ$. Chatterjee et al. (2008) give: $t_0 = 1997.59 \pm 0.11$, PA (average position angle within 1 mas of the core) $= -135^\circ \pm 4^\circ$ and apparent speed $\beta_{\rm a} = 10.1 \pm 1.2$. The fitting results are shown in Figures 3 and 4. These show that the kinematics (trajectory, core distance and apparent velocity) of knot C11 are well interpreted in terms of the precession model.

3.2 Model Fitting of the Kinematics of Knot C12

We take the following parameters: ejection epoch $t_0 = 1998.56$, precession phase $\phi = 6.22$ rad, bulk Lorentz factor $\Gamma = 21.0$, $c2 = 8$ mas and $c3 = 1200$ mas. Correspondingly we obtain: IPA $= -139.2^\circ$ and IVA $= 1.87^\circ$. Chatterjee et al. (2008) give: $t_0 = 1998.56 \pm 0.09$, PA $= -129^\circ \pm 3^\circ$ and apparent speed $\beta_{\rm a} = 16.9 \pm 0.4$.

The fitting results are shown in Figures 5 and 6. These show that the kinematics (initial trajectory, core distance and apparent velocity) of knot C12 can be well interpreted in terms of the precession model, by requiring a closer collimation/curvature at $c2 = 8$ mas.

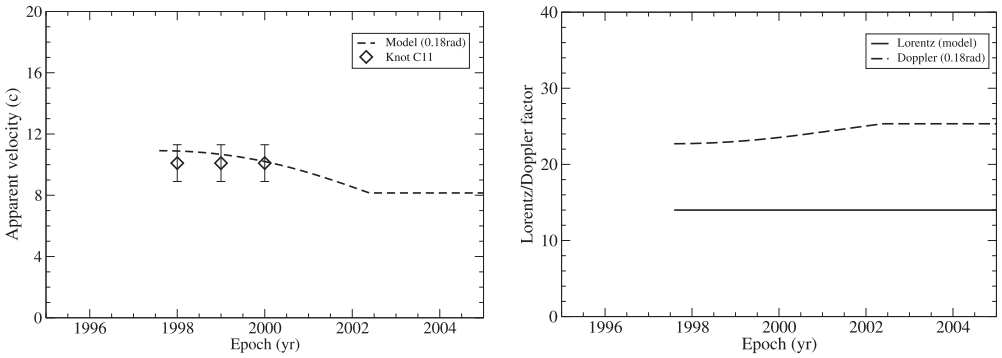

Fig. 4 Model fit of the apparent velocity (*left panel*) and Lorentz/Doppler factor from the model (*right panel*) of knot C11.

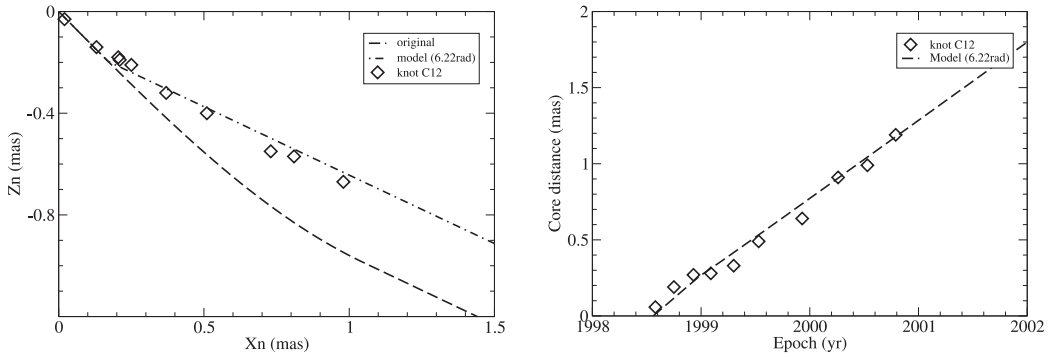

Fig. 5 Model fit of the trajectory (*left panel*) and core distance (*right panel*) of knot C12. The initial portion of the observed trajectory is well fitted by the precession model, by requiring a closer collimation/curvature at $c2 = 8$ mas. The *dashed line* in the left panel is for the original model with $c2 = b = 50$ mas.

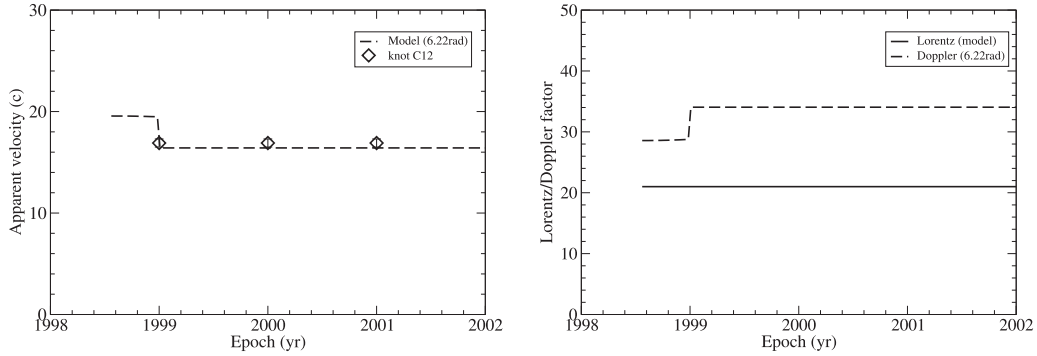

Fig. 6 Model fits of the apparent velocity (*left panel*) and the Lorentz/Doppler factor from the model (*right panel*) of knot C12.

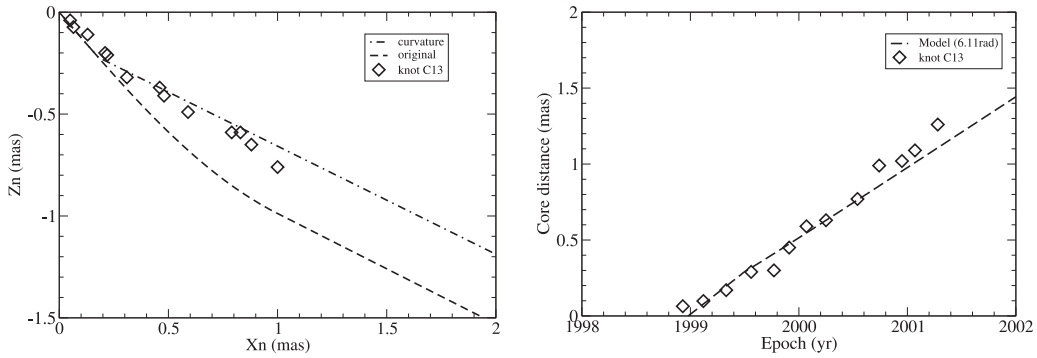

Fig. 7 Model fit of the trajectory (*left panel*) and core distance (*right panel*) of knot C13. The initial portion of the observed trajectory is well fitted by the precession model, by requiring a closer collimation/curvature at $c2 = 9$ mas. The *dashed line* in the left panel is for the original model with $c2 = b = 50$ mas.

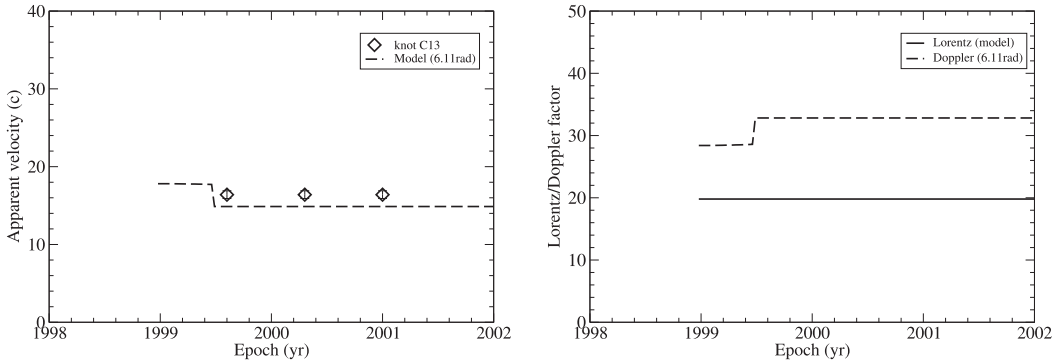

Fig. 8 Model fits of the apparent velocity (*left panel*) and the Lorentz/Doppler factor from the model (*right panel*) of knot C13.

3.3 Model Fitting of the Kinematics of Knot C13

We take the following parameters: bulk Lorentz factor $\Gamma = 19.8$, precession phase $\phi = 6.11$ rad, ejection epoch $t_0 = 1998.98$, $c2 = 9$ mas and $c3 = 500$ mas. Correspondingly we obtain: IPA $= -141.3°$ and IVA $= 1.82°$. Chatterjee et al. (2008) give: $t_0 = 1998.98 \pm 0.07$, PA $= -130° \pm 4°$ and apparent speed $\beta_{\rm a} = 16.4 \pm 0.5$. The fitting results are shown in Figures 7 and 8. The kinematics (initial trajectory, core distance and apparent velocity) are well fitted. The apparent speed derived from the model is very consistent with the observed apparent velocity given by Chatterjee et al. (2008).

3.4 Model Fitting of the Kinematics of Knot C14

We take the following parameters: precession phase $\phi = 5.98$ rad, bulk Lorentz factor $\Gamma = 22.0$, ejection time $t_0 = 1999.50$, $c2 = 12$ mas and $c3 = 500$ mas. Correspondingly we obtain: IPA

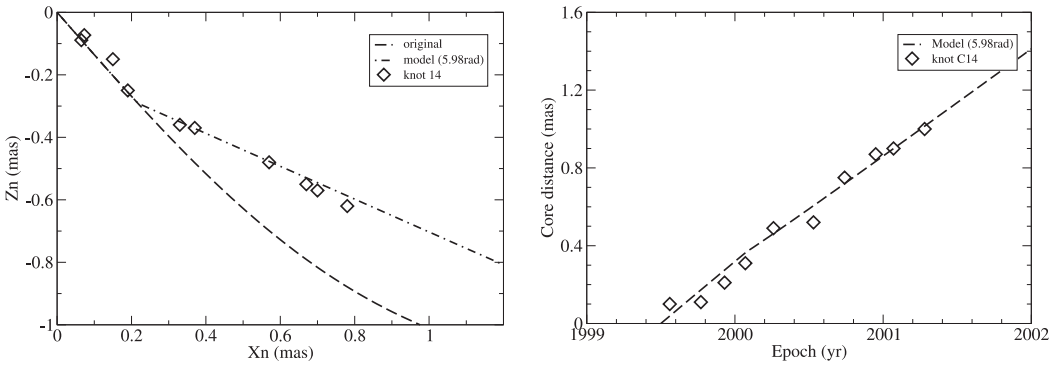

Fig. 9 Model fit of the trajectory (*left panel*) and core distance (*right panel*) of knot C14. The initial portion of the observed trajectory is well fitted by the precession model, by requiring a closer collimation/curvature at $c2 = 12$ mas. The *dashed line* in the left panel is for the original model with $c2 = b = 50$ mas.

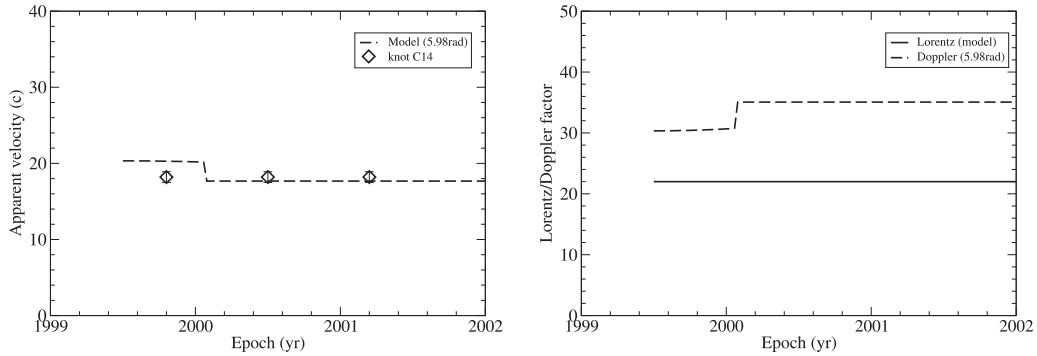

Fig. 10 Model fit of the apparent velocity (*left panel*) and the Lorentz/Doppler factor from the model (*right panel*) of knot C14. The observed apparent velocity 18.2±0.7 given by Chatterjee et al. (2008) is well fitted.

$= -143.7°$ and IVA = 1.75°. Chatterjee et al. (2008) give: $t_0 = 1999.50 \pm 0.09$, PA $= -135° \pm 6°$ and apparent speed $\beta_{\rm a} = 18.2 \pm 0.7$. The fitting results are shown in Figures 9 and 10. The kinematics of the knot (initial trajectory, core distance and apparent velocity) are well fitted by the precession model, by requiring a closer collimation/curvature at $c2 = 12$ mas.

3.5 Model Fitting of the Kinematics of Knot C15

We take the following parameters: bulk Lorentz factor $\Gamma = 20.7$, precession phase $\phi = 5.89$ rad, ejection epoch $t_0 = 1999.85$, $c2 = 10$ mas and $c3 = 500$ mas. Correspondingly we obtain: IPA $= -145.3°$ and IVA $= 1.70°$. Chatterjee et al. (2008) give: $t_0 = 1999.85 \pm 0.05$, PA $= -131° \pm 7°$ and apparent speed $\beta_{\rm a} = 17.2 \pm 2.3$. The fitting results are shown in Figures 11 and 12. It can be seen that the initial trajectory, core distance and apparent speed of knot C15 are well fitted by the precession model.

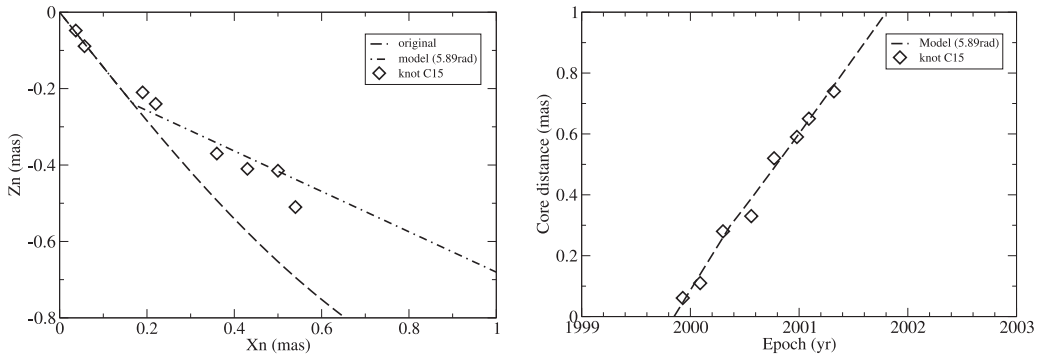

Fig. 11 Model fit of the trajectory (*left panel*) and core distance (*right panel*) of knot C15. The initial trajectory is well fitted by the precession model, by requiring a closer collimation/curvature at $c2 = 10$ mas. The *dashed line* in the left panel is for the original model with $c2 = b = 50$ mas.

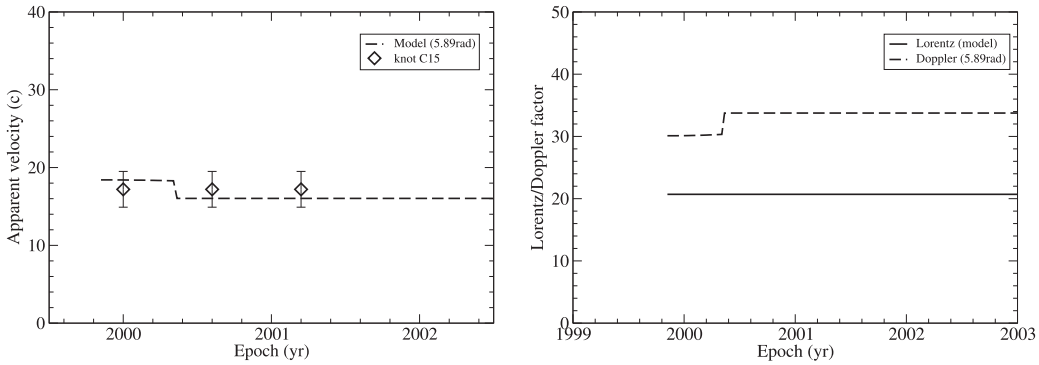

Fig. 12 Model fits of the apparent velocity (*left panel*) and the Lorentz/Doppler factor from the model (*right panel*) of knot C15. The observed apparent velocity given by Chatterjee et al. (2008) is well fitted by the precession model.

3.6 Model Fitting of the Kinematics of Knot C16

We take the following parameters: ejection epoch $t_0 = 2000.27$, precession phase $\phi = 5.79$ rad, bulk Lorentz factor $\Gamma = 20.65$, $c2 = 12$ mas and $c3 = 12\,000$ mas. Correspondingly we obtain: IPA $= -147.0°$ and IVA $= 1.63°$. Chatterjee et al. (2008) give: $t_0 = 2000.27 \pm 0.05$, PA $= -140° \pm 8°$ and apparent speed $\beta_{\rm a} = 16.9 \pm 3.5$.

The model fitting results are shown in Figures 13 and 14. The kinematics (initial trajectory, core distance and apparent speed) of knot C16 can be well fitted by the precession model with a collimation/curvature at $c2 = 12$ mas.

3.7 Model Fitting of the Kinematics of Knot C18

We take the following parameters: bulk Lorentz factor $\Gamma = 9.7$, precession phase $\phi = 5.50$ rad and ejection epoch $t_0 = 2001.40$. Correspondingly we obtain: IPA $= -151.4°$ and IVA $= 0.44°$. For knot C18 only a few points along its trajectory closest to the core are collected, thus the fit of

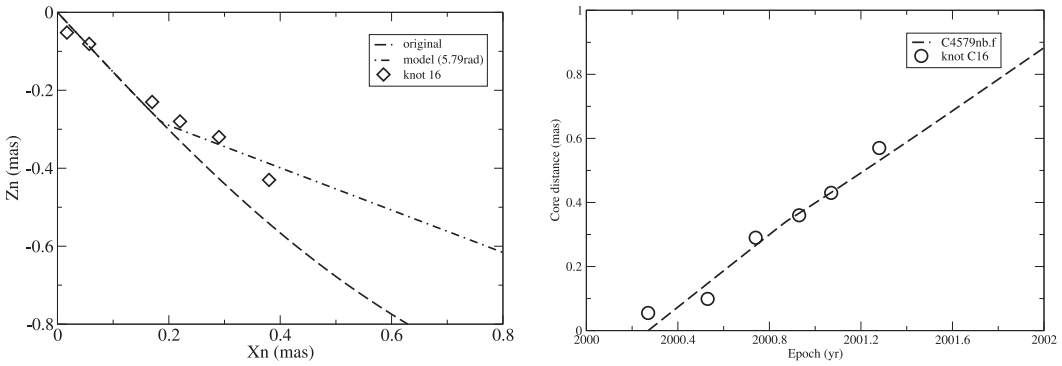

Fig. 13 Model fit of the trajectory (*left panel*) and core distance (*right panel*) of knot C16. The initial trajectory is well fitted by the precession model and a closer collimation/curvature at $c2 = 12$ mas is required. The *dashed line* in the left panel is for the original model with $c2 = b = 50$ mas.

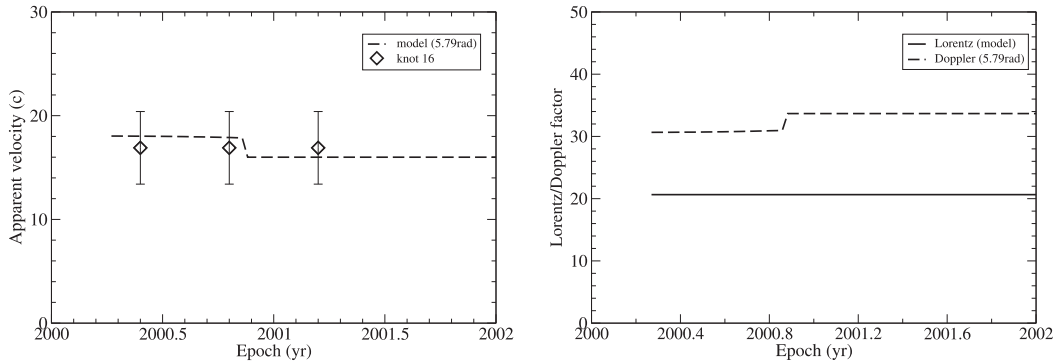

Fig. 14 Model fit of the apparent velocity (*left panel*) and the Lorentz/Doppler factor from the model (*right panel*) of knot C16.

the trajectory to the model is only for these points and the average trajectory (or average position angle) within 1 mas of the core is given by Chatterjee et al. (2008). Chatterjee et al. (2008) give: $t_0 = 2001.40 \pm 0.16$, PA $= -150^\circ \pm 8^\circ$ and apparent speed $\beta_\mathrm{a} = 4.4 \pm 0.7$. The fitted results are shown in Figures 15 and 16.

Figure 15 shows that the model fitting of the trajectory is quite good within $\sim$0.15 mas of the core. The distance from the core and apparent velocity of knot C18 can be well fitted by the precession model, especially the observed apparent velocity 4.4$\pm$0.7 given by Chatterjee et al. (2008).

3.8 Model Fitting of the Kinematics of Knot C20

We take the following parameters: ejection epoch $t_0 = 2003.39$, precession phase $\phi = 5.00$ rad and bulk Lorentz factor $\Gamma = 13.2$. Correspondingly we obtain: IPA $= -155.2^\circ$ and IVA $= 1.06^\circ$. Chatterjee et al. (2008) give: $t_0 = 2003.39 \pm 0.10$, PA $= -155^\circ \pm 10^\circ$ and apparent speed $\beta_\mathrm{a} = 6.0 \pm 0.5$.

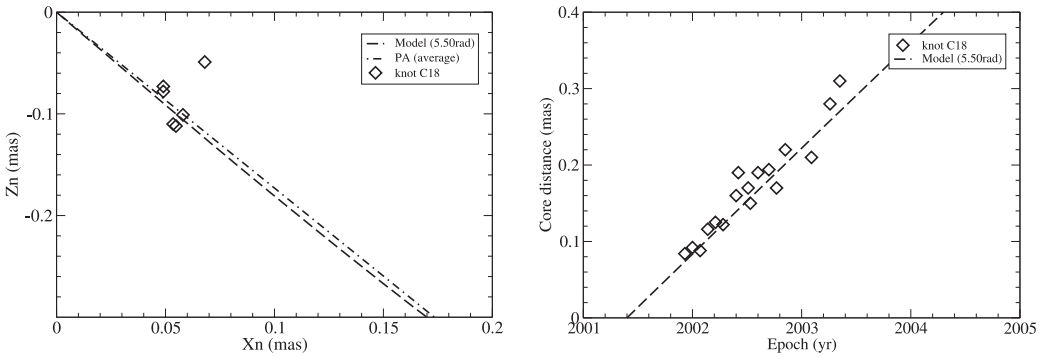

Fig. 15 Model fit of the trajectory (*left panel*) and core distance (*right panel*) of knot C18. Diamonds (*left panel*) show the observed trajectory closest to the core and the *dot-dashed line* shows the average position angle ($-150°$) within 1 mas of the core given by Chatterjee et al. (2008), which almost coincides with the modeled trajectory (*dashed line*) within $\sim$0.45 mas of the core.

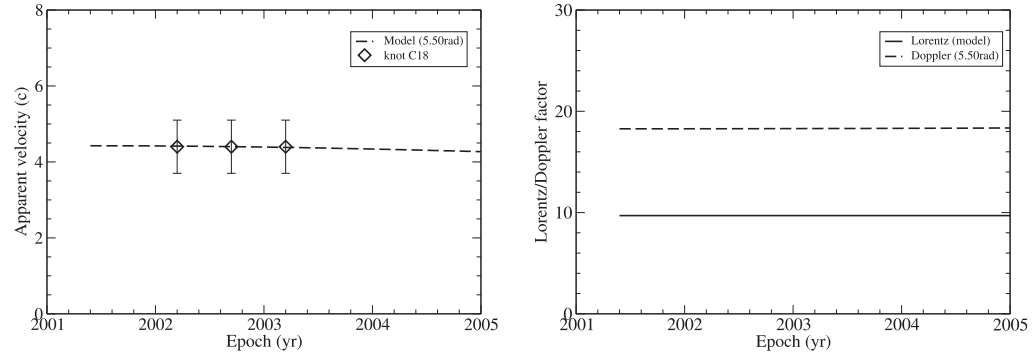

Fig. 16 Model fits to the apparent velocity (*left panel*) and the Lorentz/Doppler factor from the model (*right panel*) of knot C18.

For knot C20, only a few points along its trajectory closest to the core are collected from the literature, thus the model fitting of its trajectory is only for these points, and the average trajectory (or average position angle) within 1 mas is given by Chatterjee et al. (2008).

The fitting results are shown in Figures 17 and 18. Figure 17 (left panel) shows that the fit of the model to the trajectory is quite good for the initial part within $\sim$0.3 mas of the core. The distance from the core and apparent speed can be well fitted by the precession model, especially the observed apparent velocity given by Chatterjee et al. (2008) (Fig. 18, left panel).

3.9 Model Fitting of the Kinematics of Knot C21

We take the following parameters: ejection epoch $t_0 = 2004.75$, precession phase $\phi = 4.66$ rad and bulk Lorentz factor $\Gamma = 24.5$. Correspondingly we obtain: IPA $= -151.9°$ and IVA $= 0.80°$. Chatterjee et al. (2008) give $t_0 = 2004.75 \pm 0.05$, PA $= -147° \pm 7°$ and apparent speed $\beta_{\rm a} = 16.7 \pm 0.3$.

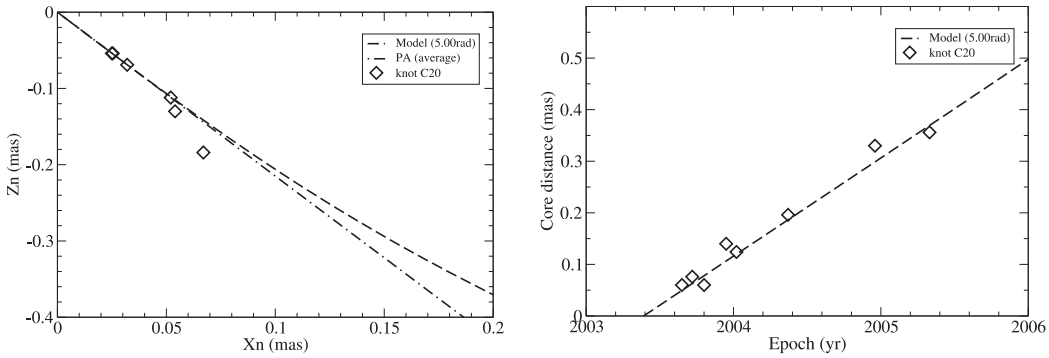

Fig. 17 Model fit of the trajectory (*left panel*) and core distance (*right panel*) of knot C20. Diamonds (*left panel*) show the trajectory closest to the core and the *dot-dashed line* represents the average position angle ($-155°$) within 1 mas of the core given by Chatterjee et al. (2008), which almost coincides with the modeled trajectory (*dashed line*) within $\sim$0.3 mas of the core.

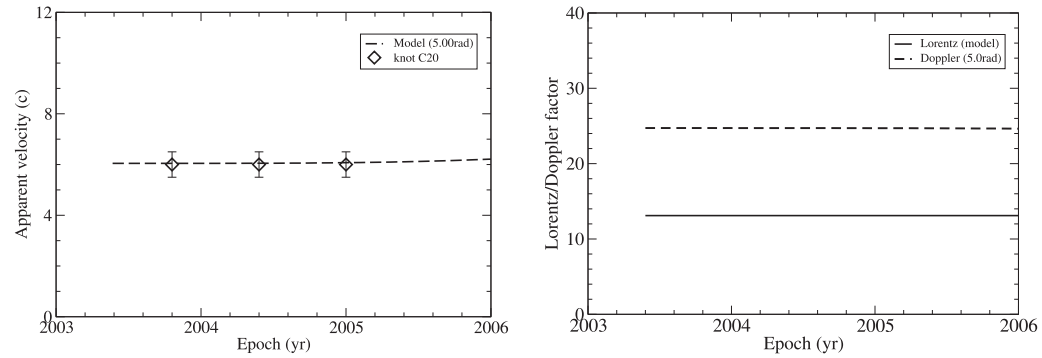

Fig. 18 Model fit of the apparent velocity (*left panel*) and the Lorentz/Doppler factor from the model (*right panel*) of knot C20.

For knot C21, only a few points along its trajectory closest to the core are collected, thus the model fitting of its trajectory is only for these points, and the average trajectory (or average position angle) within 1 mas of the core is given by Chatterjee et al. (2008). The fitting results are shown in Figures 19 and 20. It can be seen that the model fitting of the trajectory is quite good within a core distance of $\sim$0.3 mas. The core distance and apparent velocity of knot C21 are well fitted by the precession model.

3.10 Model Fitting of the Kinematics of Knot C24

We take the following parameters: ejection epoch $t_0 = 2006.74$, precession phase $\phi = 4.16$ rad and bulk Lorentz factor $\Gamma = 26.0$. Correspondingly we obtain: initial position angle IPA $= -126.0°$ and initial viewing angle IVA $= 0.54°$. Larionov et al. (2008) give: $t_0 = 2006.89 \pm 0.11$, PA $=\sim -122.6° \pm 4°$ (Jorstad, private communication) and apparent speed $\beta_{\rm a} = 14.7 \pm 0.9$. The fitting results are shown in Figures 21 and 22. It can be seen that the kinematics (trajectory, core distance and apparent velocity) of knot C24 can be well fitted by the precession model.

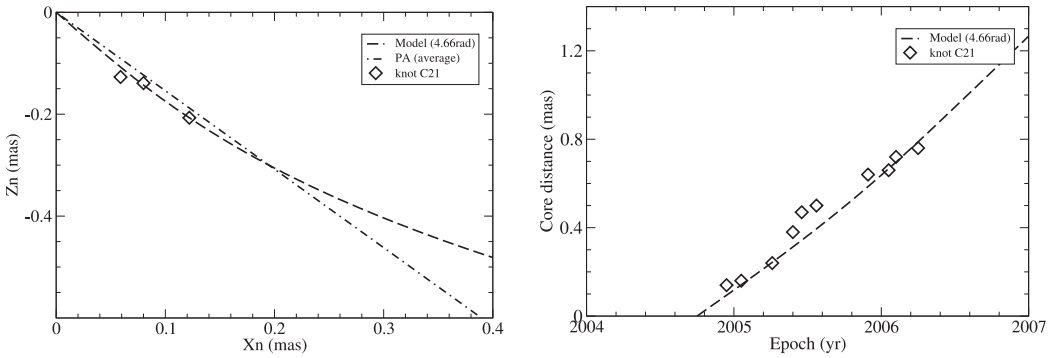

Fig. 19 Model fit of the trajectory and core distance of knot C21. Diamonds (*left panel*) show the trajectory closest to the core. The *dot-dashed line* represents the average position angle (-147°) within 1 mas of the core given by Chatterjee et al. 2008, which closely coincides with the modeled trajectory (*dashed line*) within $\sim$0.3 mas of the core.

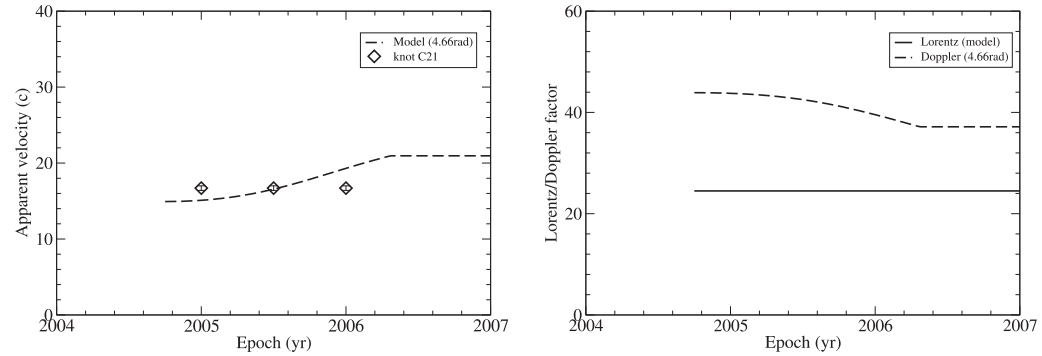

Fig. 20 Model fit of the apparent velocity (*left panel*) and the Lorentz/Doppler factor from the model (*right panel*) of knot C21.

4 DISCUSSION

We have fit the kinematics to the model of ten superluminal components (C11–C16, C18, C20, C21 and C24) for blazar 3C 279 in terms of the precession scenario proposed in Qian (2011). It is found that their initial trajectory (i.e. initial/ejection position angles)[3], core distances and apparent speeds observed by the VLBI observations can be well explained by the model. Thus, combined with the six components well fitted in Qian (2012), now sixteen superluminal components (about $\sim$60% of the total number of superluminal components) can be consistently well interpreted by the precession model. The remaining 40% of the superluminal components include knots C5a, C6, C7, C17, C19, C22 and C23. The observed initial trajectory (or ejection/IPA) for these knots significantly deviates from those predicted by the precession model, as shown in figure 14 in Qian (2011).

[3] As we pointed out before, here "initial trajectory" means "the portion of the trajectory within a core distance of $\sim$0.2–0.4 mas." Thus the corresponding IPA is regarded as the ejection position angle to be fitted by the precession model. The "average" position angle within 1 mas of the core given by e.g. Chatterjee et al. 2008 is often different from the IPA." That is why the "average position angle" of C12 to C16 cannot be fitted by the precession model (see Fig. 24 (left panel)), but their IPA can be fitted by the precession model with a 25 year period, as shown in Figure 24 (left panel).

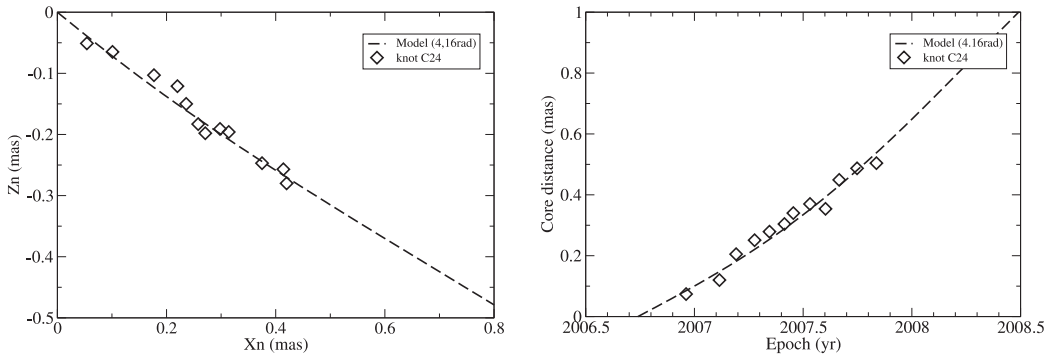

Fig. 21 Model fit of the trajectory (*left panel*) and core distance (*right panel*) of knot C24.

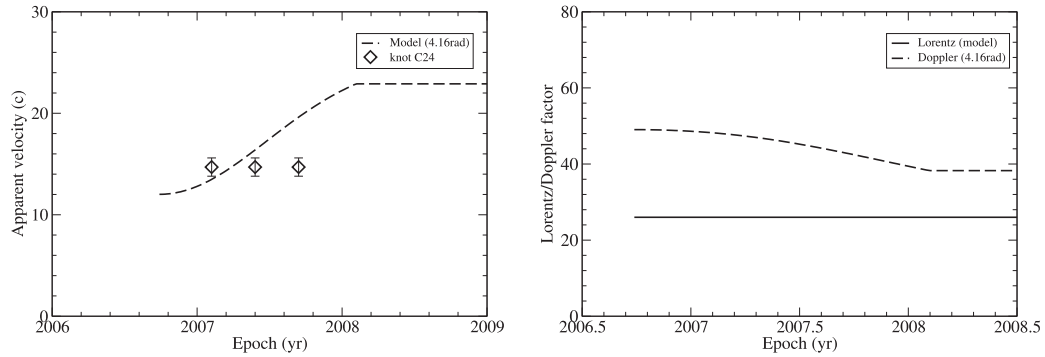

Fig. 22 Model fit of the apparent velocity (*left panel*) and the Lorentz/Doppler factor from the model (*right panel*) of knot C24.

In a separate paper we will discuss how to interpret the kinematics of these components in terms of the precession scenario.

We summarize the parameters from the model fit (ejection time t_0, precession phase ϕ, bulk Lorentz factor Γ, IPA and IVA) for the ten superluminal components (C11–C16, C18, C20, C21 and C24) in Table 2. It is remarkable that all the ejection times of the components adopted in the model are very consistent with the values derived from the VLBI observations.

In other words, the ejection times derived from the VLBI observations are very consistent with the precession phase of the 25 year period. From Figures 3–22 it can be seen that the fitting results of trajectory, core distance and apparent velocity are good for all ten knots.

Figure 23 (left panel) shows a comparison of the model fits for the trajectory of knots C11 and C24, clearly demonstrating the precession of trajectory in the period 1997.59–2006.74 with the precession phase differing by about 2.3 rad (corresponding to a time span of $\Delta t_0 = 9.15$ yr). In Figure 23 (right panel) is shown the comparison of the model fits for the trajectory of knots C16 and C24, also demonstrating the precession of the initial trajectory during the period 2000.27–2006.74 with the precession phase differing by about 1.63 rad (time coverage of $\sim$6.5-yr). Combining the results shown in Figure 23, Figure 1 (right panel) and the fitting results in this paper, we might suggest that the ejections of the superluminal components fitted here are related to a possible jet precession.

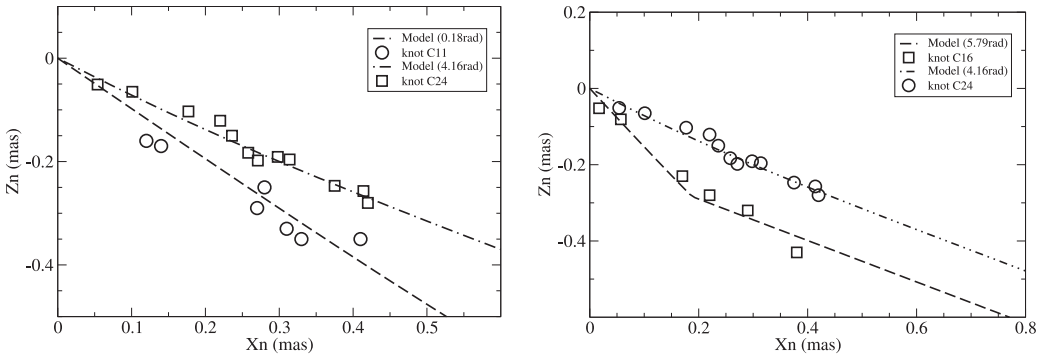

Fig. 23 Comparison of the trajectory model fits for knots C11 and C24 (about 9 yr separation, *left panel*) and the trajectory model fits for knots C16 and C24 (about 6.5 yr time separation, *right panel*), showing the possible precession in the jet.

Table 2 Model Parameters for the Ten Superluminal Components

Knot	t_0	ϕ (rad)	Γ	IPA (°)	IVA (°)	$t_{0,\mathrm{VLBI}}$	$\mathrm{PA_{VLBI}}$ (°)
(1)	(2)	(3)	(4)	(5)	(6)	(7)	(8)
C11	1997.59	0.18	14.0	–134.3	1.97	1997.59±0.11	–135±4
C12	1998.56	6.22	21.0	–139.2	1.87	1998.56±0.09	–129±3
C13	1998.98	6.11	19.8	–141.3	1.82	1998.98±0.07	–130±4
C14	1999.50	5.98	22.0	–143.7	1.75	1999.50±0.09	–135±6
C15	1999.85	5.89	20.7	–145.3	1.70	1999.85±0.05	–131±7
C16	2000.27	5.79	20.65	–147.0	1.63	2000.27±0.05	–140±8
C18	2001.40	5.50	9.7	–151.4	1.44	2001.40±0.16	–150±8
C20	2003.39	5.00	13.2	–155.2	1.06	2003.39±0.05	–155±10
C21	2004.75	4.66	24.5	–151.9	0.80	2004.75±0.05	–147±7
C24	2006.74	4.16	26.0	–126.0	0.54	2006.89±0.11	–123±4

Notes: Column (1) is knot number, Col. (2) ejection epoch, Col. (3) precession phase, Col. (4) bulk Lorentz factor, Col. (5) and Col. (6) are IPA and IVA. For comparison, $t_{0,\mathrm{VLBI}}$ and $\mathrm{PA_{VLBI}}$ are taken from Chatterjee et al. (2008) and Larionov et al. (2008).

Figure 24 shows the relation between the IPA and the ejection epoch (left panel) and the relation between the IPA and the IVA (right panel). In the latter it shows that the viewing angle changes in the range $\sim 0.5^\circ - 2^\circ$, which is consistent with the estimates derived by Jorstad et al. (2004).

Figure 25 shows the relation, derived from the model, between the bulk Lorentz factor and the precession phase (left panel) and the IPA (right panel).

Figure 26 shows the relation between bulk Lorentz factor and the IVA (left panel) and that between the bulk Lorentz factor and the ejection time (right panel). The modeled Lorentz factor is in the range of $\sim$10 to 30, which is mostly consistent with the estimates derived by Jorstad & Marscher (2005).

Jorstad & Marscher (2005) pointed out that the different apparent superluminal velocities observed for different components in 3C 279 might be explained by the precession of the jet with constant Lorentz factor, but two or more periods are needed to confirm this. Our results, which represent more than one period and are derived from detailed fittings to the model, are shown in Figures 25 and 26. The bulk Lorentz factors derived for different components do not show any regular trend. Since these Lorentz factor values are derived from the consistent fits of the model to the trajecto-

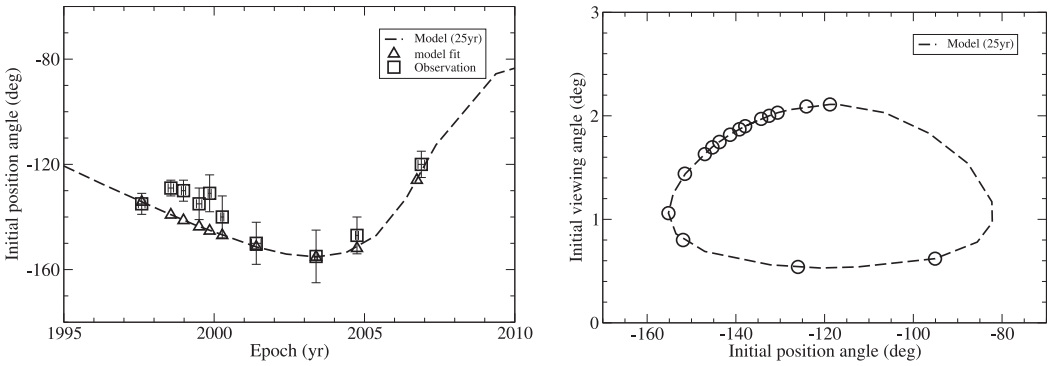

Fig. 24 *Left panel*: Relation between the IPA and ejection time for ten knots (C11– C16, C18, C20, C21 and C24): model fits (*triangles*) and observed average position angle (*squares*, Chatterjee et al. 2008). *Right panel*: Model fitting relation between IPA and IVA for the sixteen knots (C3, C4, C7a, C8–C16, C18, C20, C21 and C24). The viewing angle derived by the precession model is in the range of $0.5^\circ - 2^\circ$, which is remarkably consistent with the estimates given by Jorstad et al. (2004).

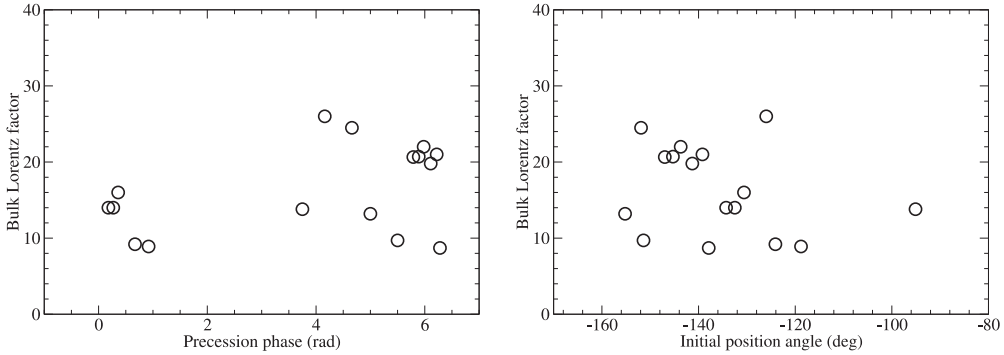

Fig. 25 Relations between bulk Lorentz factor and precession phase (*left panel*), and IPA (*right panel*). The modeled Lorentz factor is in the range of $\sim$10 to 30, which is mostly consistent with the estimates derived by Jorstad & Marscher (2005).

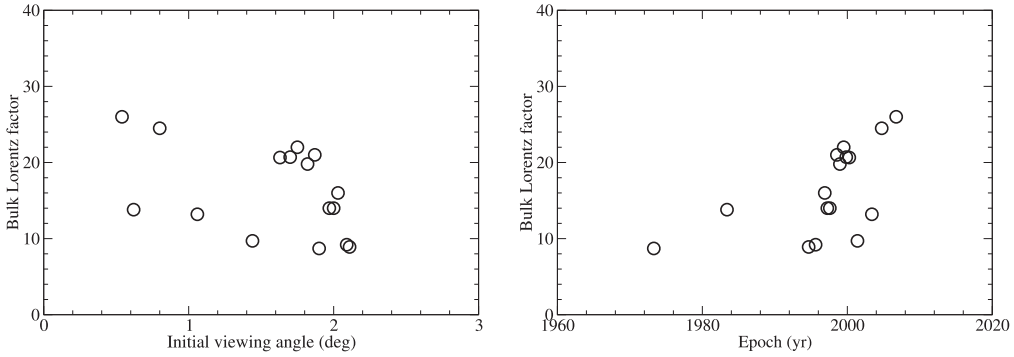

Fig. 26 Relations between bulk Lorentz factor and IVA (*left panel*), and ejection time (*right panel*).

ries, distances from the core and apparent velocities observed by VLBI observations, they should be regarded as well determined. This seems to imply that the observed apparent speeds are not simply dependent on the change in the viewing angle with a constant Lorentz factor that is produced from precession. In other words, it seems that the bulk Lorentz factor for knots probably mainly depends on the activity in the central engine (black hole/accretion disk system, and the efficiency of the energy transfer to the jet), which could vary non-regularly.

5 CONCLUSIONS

In this paper we have fit a model to the kinematics of ten superluminal components (C11–C16, C18, C20, C21 and C24) in 3C 279 in terms of the precession scenario proposed by Qian (2011). Combined with the model fitting to the kinematics of six components (C3, C4 C7a, C8, C9 and C10) already published in Qian (2012), now there are sixteen components for which their initial trajectory (or ejection/IPA), distance to the core and apparent speed observed by VLBI observations can be consistently well explained by the precession model with a period of 25 yr proposed in Qian (2011). In the process of fitting to the model, we find that the precession scenario, used to interpret the kinematic behavior (or pattern of trajectories) of the superluminal knots, mainly depends on three ingredients: ejection by precession, initial collimation and curvature at the outer distance. Thus on the whole, we have found three classes of trajectories for the superluminal knots in blazar 3C 279, which are described as follows.

(1) In the original model proposed by Qian (2011), the amplitude function describing the trajectory is given by Equations (1) and (2) of that paper with the collimation parameter $b = 50$ mas. Typical trajectories which can be explained in terms of the original amplitude function are those from knots C9 and C4. The model fits of their trajectory are shown in Figure 1 (right panel) with their ejection time spanning 13.5 yr, demonstrating the difference in their ejection position angle of 35.5° due to precession. In addition, for knot C4 a curvature in the trajectory occurs at axial distance $z \simeq 160$ mas. We point out that the distance to the core and apparent speed observed for both knots C4 and C9 are very well fitted (see fig. 4 (for C4) and fig. 16 (for C9) in Qian 2012). Especially for knot C4, the derived change in viewing angle, Doppler factor and apparent speed are remarkably consistent with the analysis of the VLBI observations by Homan et al. (2003). Moreover, the decrease in flux density of C4 after the curvature can be understood by taking into account the increase in its angular size and the decrease in its Doppler factor.
(2) For six knots (C3, C7a, C8, C10, C11 and C24), their trajectories are observed to be basically ballistic (linear) and thus collimation/curvature in their trajectory cannot be determined. Their kinematics (trajectory, distance to the core and apparent speed) are well fitted in terms of the original precession model. Knots C18, C20 and C21 might also belong to this class.[4]
(3) As shown by the results of the model fitting in this paper, the initial trajectory of five knots (C12, C13, C14, C15 and C16) can be well fitted within projected distance to the core of less than about 0.2–0.3 mas. This requires the collimation parameter ($c2$) of their amplitude function to be in the range $\sim$8 mas to 12 mas. Thus these knots have collimation much closer than knots C4 and C9, but their initial trajectory can still be explained by the precession model. The model fitting of their distance to the core and apparent speed are also quite good as demonstrated in this paper.

For all three classes of knots listed above, their VLBI kinematics (initial trajectory, distance to the core and apparent speed) can be consistently interpreted in terms of our precession model. Although only part of the superluminal components of 3C 279 ($\sim$60%) is explained and the precession model has yet to be tested by future observations, our analysis may be useful to understand the

[4] For these knots more data on position angle are needed to make a certain identification of class.

behavior of superluminal knots in blazar 3C 279 from VLBI observations, by helping to disentangle different mechanisms and ingredients.

In a companion paper (Qian, in preparation) we will show that, in order to fit the kinematics of another seven knots (C5a, C6, C7, C17, C19, C22 and C23) in terms of the precession scenario, collimation of their trajectory at axial distance $c2 \simeq 1-3$ mas and some curvature in the trajectory are required. This could be regarded as a fourth class of knots. Under this assumption, their kinematics (the observed part of the trajectory, distance to the core and apparent speed) could still be interpreted in terms of the precession model. Since the assumed collimation of their trajectory occurs much closer to the core (even closer than that for knots C12 to C16), current VLBI observations cannot resolve this part of their trajectory (within $\sim$0.05 mas). Thus tests would be required for future higher resolution VLBI observations. In addition, we will also discuss the possibility of explaining the VLBI kinematics of these knots with a binary jet scenario.

Considering the complex kinematics of the superluminal components in blazar 3C 279, combined with different bulk Lorentz factors for different knots, we would think that the scenario of a precession jet model proposed by Qian (2011) may be useful for helping to understand the physics of its relativistic jet, by disentangling different mechanisms and ingredients. Different trajectory patterns of the knots with collimation at an axial distance of $\sim$50, $\sim$10 and $\sim$2 mas in the precession scenario might reflect the patterns of a helical magnetic field near the core (or nozzle) which evolve with time. It seems that some regular pattern of initial trajectory (or a rotating channel) could exist in 3C 279. This kind of steady rotating channel, if it really exists, must be strongly related to the magnetic structure of the central engine (Meier & Nakamura 2006; McKinney 2006; Vlahakis & Koenigl 2004; Meier 2001; Meier et al. 2001). Jet precession could be related to binary black hole systems as one of the plausible mechanisms (Britzen et al. 2001; Karouzos et al. 2011; Kudryavtseva et al. 2011).

Acknowledgements I wish to thank Dr. Jorstad (Boston University, USA) for providing the VLBI data for knots C23 and C24.

References

Abdo, A. A., Ackermann, M., Agudo, I., et al. 2010, ApJ, 716, 30
Agudo, I., Bach, U., Krichbaum, T. P., et al. 2007, A&A, 476, L17
Bach, U., Krichbaum, T. P., Ros, E., et al. 2005, A&A, 433, 815
Britzen, S., Roland, J., Laskar, J., et al. 2001, A&A, 374, 784
Carrara, E. A., Abraham, Z., Unwin, S. C., & Zensus, J. A. 1993, A&A, 279, 83
Chatterjee, R., Jorstad, S. G., Marscher, A. P., et al. 2008, ApJ, 689, 79
Chatterjee, R., Bailyn, C. D., Bonning, E. W., et al. 2012, ApJ, 749, 191
Cohen, M. H., Cannon, W., Purcell, G. H., et al. 1971, ApJ, 170, 207
Hartman, R. C., Bertsch, D. L., Fichtel, C. E., et al. 1992, ApJ, 385, L1
Hogg, D. W. 1999, arXiv: astro-ph/9905116
Homan, D. C., Lister, M. L., Kellermann, K. I., et al. 2003, ApJ, 589, L9
Jorstad, S. G., Marscher, A. P., Lister, M. L., et al. 2004, AJ, 127, 3115
Jorstad, S. G., & Marscher, A. P. 2005, Mem. Soc. Astron. Italiana, 76, 106
Jorstad, S. G., Marscher, A. P., Stevens, J. A., et al. 2007, AJ, 134, 799
Jorstad, S., Marscher, A., Smith, P., et al. 2012, International Journal of Modern Physics Conference Series, 8, 356
Karouzos, M., Britzen, S., Witzel, A., Zensus, J. A., & Eckart, A. 2011, A&A, 529, A16
Kudryavtseva, N. A., Britzen, S., Witzel, A., et al. 2011, A&A, 526, A51
Larionov, V. M., Jorstad, S. G., Marscher, A. P., et al. 2008, A&A, 492, 389
Lobanov, A. P., & Roland, J. 2005, A&A, 431, 831

Marscher, A. P. 2008, in ASPC 386, Extragalactic Jets: Theory and Observation from Radio to Gamma Ray, eds. T. A. Rector, & D. S. De Young, 437
Marscher, A. P. 2009, in ASPC, 402, Approaching Micro-Arcsecond Resolution with VSOP-2: Astrophysics and Technologies, eds. Y. Hagiwara, E. Fomalont, M. Tsuboi, & M. Yasuhiro, 194
Marscher, A. P., Jorstad, S. G., Larionov, V. M., et al. 2010, ApJ, 710, L126
Marscher, A., Jorstad, S. G., Larionov, V. M., Aller, M. F., & Lähteenmäki, A. 2011, Journal of Astrophysics and Astronomy, 32, 233
Marscher, A. P., & Jorstad, S. G. 2011, ApJ, 729, 26
Marscher, A. P., Jorstad, S. G., Agudo, I., MacDonald, N. R., & Scott, T. L. 2012, arXiv:1204.6707
McKinney, J. C. 2006, MNRAS, 368, 1561
Meier, D. L. 2001, ApJ, 548, L9
Meier, D. L., Koide, S., & Uchida, Y. 2001, Science, 291, 84
Meier, D. L., & Nakamura, M. 2006, in ASPC 350, Blazar Variability Workshop II: Entering the GLAST Era, eds. H. R. Miller, K. Marshall, J. R. Webb, & M. F. Aller, 195
Pen, U.-L. 1999, ApJS, 120, 49
Qian, S. J., Witzel, A., Krichbaum, T., et al. 1992, Chinese Astronomy and Astrophysics, 16, 137 (original version: Qian, S. J., Witzel, A., Krichbaum, T., Quirrenbach, A., Hummel, C. A., Zensus, J. A., 1991, Acta Astron. Sin. 32, 369)
Qian, S. J., Krichbaum, T. P., Zensus, J. A., Steffen, W., & Witzel, A. 1996, A&A, 308, 395
Qian, S.-J., Witzel, A., Zensus, J. A., et al. 2009, RAA (Research in Astronomy and Astrophysics), 9, 137
Qian, S.-J., Krichbaum, T. P., Witzel, A., et al. 2010, RAA (Research in Astronomy and Astrophysics), 10, 47
Qian, S.-J. 2011, RAA (Research in Astronomy and Astrophysics), 11, 43
Qian, S.-J. 2012, RAA (Research in Astronomy and Astrophysics), 12, 46
Raiteri, C. M., Villata, M., Bruschini, L., et al. 2010, A&A, 524, A43
Savolainen, T., Wiik, K., Valtaoja, E., & Tornikoski, M. 2006, A&A, 446, 71
Schinzel, F. K., Lobanov, A. P., Jorstad, S. G., et al. 2010, in Proceedings of the Workshop “Fermi meets Jansky - AGN in Radio and Gamma-Rays”, eds. T. Savolainen, E. Ros, R. W. Porcas, & J. A. Zensus, MPIfR, Bonn, June 21-23 2010 (arXiv:1012.2820)
Spergel, D. N., Verde, L., Peiris, H. V., et al. 2003, ApJS, 148, 175
Steffen, W., Zensus, J. A., Krichbaum, T. P., Witzel, A., & Qian, S. J. 1995, A&A, 302, 335
Stirling, A. M., Cawthorne, T. V., Stevens, J. A., et al. 2003, MNRAS, 341, 405
Unwin, S. C., Cohen, M. H., Hodges, M. W., Zensus, J. A., & Biretta, J. A. 1989, ApJ, 340, 117
Vercellone, S., D’Ammando, F., Vittorini, V., et al. 2010, ApJ, 712, 405
Vlahakis, N., & Königl, A. 2004, ApJ, 605, 656
Wehrle, A. E., Piner, B. G., Unwin, S. C., et al. 2001, ApJS, 133, 297
Whitney, A. R., Shapiro, I. I., Rogers, A. E. E., et al. 1971, Science, 173, 225